Design and Implementation of Closed TEM Cells: Simulation-Based Approach

Vojtech BEDNARSKY, Zbynek RAIDA, Jiri DRINOVSKY

Dept. of Radio Electronics, Brno University of Technology, Technicka 12, 616 00 Brno, Czechia

{203399, raida, drino}@vut.cz

Submitted October 14, 2022 / Accepted February 11, 2023 / Online first March 13, 2023

Abstract. *In the paper, a simulation-based design procedure for the implementation of a TEM (Crawford) cell is presented. The empirical approach uses computer simulations carried out in CST Microwave Studio to design the cell that operates in the frequency range from 100 kHz to 400 MHz. Following the developed procedure, the TEM cell was implemented and tested experimentally. The TEM cell can be used for electromagnetic susceptibility (EMS) measurements, where the device under test (DUT) is irradiated by the field in a wide range of frequencies. The DUT is tested to operate without the performance degradation under the influence of electromagnetic disturbances. In addition, the cell can be used for electromagnetic interference (EMI) measurements focused on interference emissions generated by the DUT.*

Keywords

Transversally electromagnetic (TEM) cell, TEM waveguide mode, electromagnetic compatibility (EMC), Crawford cell, CST Microwave Studio, electromagnetic susceptibility (EMS), electromagnetic interference (EMI)

1. Introduction

For electromagnetic compatibility (EMC) testing, anechoic chambers can be used those are not affordable generally, and testing is expensive. As an alternative, TEM cells can be exploited for EMC pretesting or home tests. TEM cells can provide similar results as shown in the paper.

Transversally electromagnetic (TEM) cells are constructed to excite a uniform and homogeneous TEM wave propagating inside the structure. Often, cells operate as 50 Ω customized systems [1], [2].

TEM cells are constructed from TEM transmission lines. There are several types of TEM transmission lines. E.g., a parallel plate waveguide consists of a signal plate and a ground plate that is not connected to a center conductor (septum). If septum is added, the transmission line (a conventional TEM cell) shows better load matching. Due to the inserted septum, the height of the device under test (DUT) must be lower compared to the waveguide of the parallel plate, keeping the same overall geometry [1], [2].

As depicted in Fig. 1, the TEM cell can be seen as a rectangular coaxial line with a planar inner conductor and air filling. For a particular line, the signal conductor is led from the connector to the inner center conductor (septum). The outside conductors are connected to the ground. The input and output sections are tapered to ensure constant characteristic impedance along the TEM cell [3].

TEM cells are mainly used to measure electromagnetic emissions and electromagnetic immunity of electronic devices. Thanks to their size, simple construction and low purchase price, the TEM cell is a suitable alternative for measurements in anechoic chambers [1], [2].

If side walls of the waveguide are removed, an open TEM cell is obtained. When selecting between open and closed cells, following consequences should be considered:

- If emissions are measured, the effect of the background noise is suppressed by the closed TEM cell.
- For immunity testing, a closed cell is safer for operator.
- An open TEM cell is easier to be manufactured, and there is no need to make a hole for handling the DUT.
- Electromagnetic interferences (EMI) are measured with a higher accuracy in a closed TEM cell.

In an open literature, attention is mainly turned to:

- Increasing the bandwidth of strip line cells [7]. Using the presented approach, a multi-objective optimization of cells can be applied on geometry, dimensions, and construction materials.
- Analysis of higher-order modes excited in cells [8]. Exploiting fully parametric CST models, shape synthesis can be run to suppress higher-order modes. Hence, not only the modal analysis but also the modal synthesis can be performed.
- Field calibrations in cells [9], since the calibration of the field probe directly influences the uncertainty of radiated immunity tests. A parametric numerical model can help us to properly design a field probe and the calibration procedure.

DOI: 10.13164/re.2023.0177

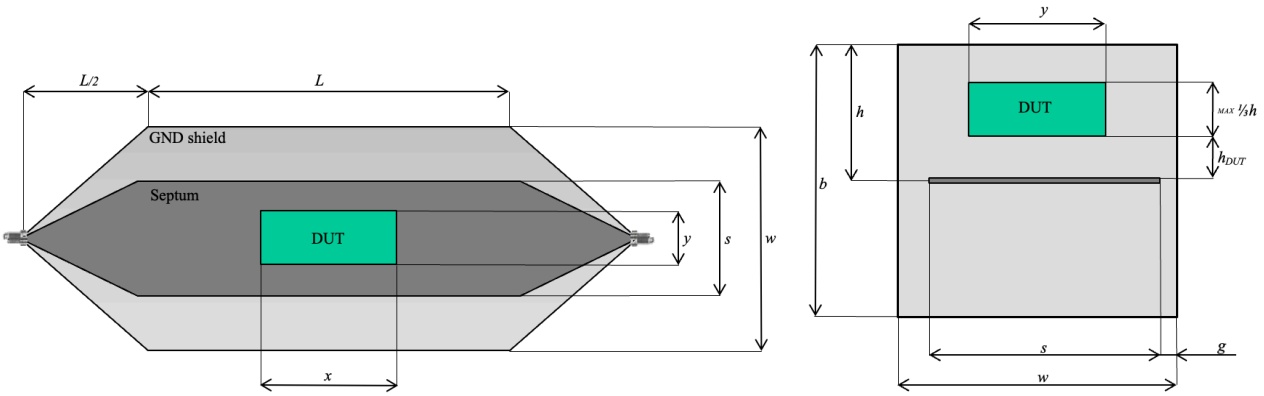

Fig. 1. The TEM cell. Left: top view. Right: inner view with a device under test.

- Proper composition of tests within TEM cells. Using a reliable numerical model of a cell, virtual prototypes of broadband couplers [10] and other components used for cell measurements can be developed.

In the open literature, exploitation of numerical models for the design of TEM cells is described in several papers. The articles investigate the methods for suppressing higher order modes in TEM cells [4], [14]. Numerical methods are used in the design phase to achieve the requested behavior of the TEM cell over a wide frequency range [15]. The accuracy of the computational model is analyzed by comparing experimental dosimetry results with computed ones comprising five liquid samples undergoing an exposure inside the TEM cell in thermal regime [16]. Using a numerical method, the responses of a short dipole probe to a calculated non-uniform E field can be evaluated [17].

Nevertheless, papers on a numerical prototyping of TEM cells in CST Microwave Studio are quite rare and incomprehensive [11], [12]. Moreover, the published models have never been experimentally verified. Therefore, a comprehensive empirical modelling approach is presented in the paper, and its validity is experimentally verified.

In Sec. 2, all relevant steps of the TEM cell design are described. As a result, the optimum parameters of a cell are obtained. In Sec. 3, numerical simulations of the TEM cell in CST Microwave Studio are presented. Thanks to the numerical model, the TEM cell can be optimized. In Sec. 4, manufacturing details are provided. Section 5 presents measurement results and their comparison with simulations. Section 6 concludes the paper.

2. TEM Cell Design

The empirical approach to the TEM cell design is illustrated by the following example:

- Operating frequencies in the range from 100 kHz to 400 MHz are covered.
- A homogeneous E-field with an intensity of up to 250 V/m is excited.
- The TEM cell is portable in shape and size.
- The TEM cell can measure electromagnetic emissions and electromagnetic immunity.
- The maximum DUT size is 0.2 m × 0.2 m × 0.1 m ($x \times y \times h_{\mathrm{DUT}}$).

The maximum size of the area for placing the DUT is limited by the space, which can be calculated from the formulas:

- $x = 0.6\ L$,
- $y = 0.4\ w$.

The DUT shall be located inside the TEM cell at a height of

- $h_{\mathrm{DUT}} = 0.3\ h$

and shall be supported by a dielectric support ($\varepsilon_{\mathrm{r}} \leq 1.4$) as shown in Fig. 1 [3], [4].

To ensure correctness of measurements, a single TEM mode has to propagate along the transmission line. With increasing frequency, relevant TE modes (TE_{01}, TE_{10}) start to propagate along the line [4]. The cut-off frequency of the TE_{01} mode can be calculated according to [4]:

$$f_{\mathrm{c,TE01}} = \frac{150}{\pi}\frac{x}{h} \tag{1}$$

where

$$x = \tan^{-1}\left(X\right), \tag{2}$$

$$X = \frac{\pi h}{w}\left[\ln\left(\frac{w}{\pi g}\right) + R_{\mathrm{TE01}}\right], \tag{3}$$

$$R_{\mathrm{TE01}} = \sum_{p=1}^{\infty}\left[\frac{1}{p}\coth\left(\frac{\pi h}{0.5w} - 1\right)\cos\left(\frac{\pi g}{0.5w}\right)\right]. \tag{4}$$

In the above equations, the parameter w is the width and b is the overall height of the TEM cell. In the formula

- $b = 2h$,

the symbol h is the height between the signal strip and the top (bottom) strip. The parameter g can be calculated from:

- $g = 0.5\ (w - s)$

where s is the septum width. The structure of the closed TEM cell with all dimensions used is depicted in Fig. 1.

Simulations in CST Microwave Studio showed that the first resonant mode TE_{01} has a short resonant peak, but the TEM cell can be used after the cut-off frequency of the TE_{10} mode. The working frequency is recommended to differ significantly from this resonant frequency [1], [5].

Some publications recommend to calculate the frequency of the first resonant mode from [3]:

$$f_{\mathrm{c,TE01}} = \frac{c}{2w}. \tag{5}$$

Here, c is the speed of light and w is the width of the TEM cell (see Fig. 1).

If the frequency is above the resonance, the impedance matching of the TEM cell deteriorates. The right choice of w affects the overall behavior of the cell [3].

In the first step, the initial parameter w is recommended to be chosen from the cut-off formula (1). To obtain other parameters, the ratio formulas are used:

- $w/L = 1.00$,
- $w/b = 1.00$,
- $w/s = 1.50$.

The initial results will be further optimized. From [2]

$$Z_0 = \frac{30\pi}{\frac{w}{b} - \frac{2}{\pi}\ln\left(\sinh\frac{\pi g}{b}\right)}, \tag{6}$$

we can calculate the characteristic impedance of the TEM cell. If a 50 Ω impedance is to be reached, a matching connected to the N-connector of the TEM cell must be used. The choice of parameters w (the width of the cell), g (the gap between the side wall and the inner conductor) and b (the height of the cell) affect the impedance matching of the TEM cell. The length of the non-tapered part of the TEM cell L influences the number of half waves inside [3], [1].

In this paper, (1) to (6) are used for the practical design of a cell. Considering initial dimensions, a numerical model of the cell is built in CST. This approach allows the designer to calibrate the numerical model according to the output of the measurements, perform sensitivity and tolerance analyses and modify the design.

To evaluate the initial design, the TEM cell with the dimensions shown in Tab. 1 was modelled in CST.

3. Simulation of the TEM Cell

First, simulations of the designed TEM cells were carried out in the frequency range from 100 kHz to 400 MHz while the main effort was aimed to obtain the best constant transmission factor characteristics. For the optimization, we used the parametric sweep.

parameter	optimized	initial
L [m]	0.400	0.500
w [m]	0.500	0.500
s [m]	0.365	0.330
b [m]	0.500	0.375
g [m]	0.068	0.085
x [m]	0.240	0.300
y [m]	0.200	0.200
h_{DUT} [m]	0.075	0.062

Tab. 1. Initial dimensions of the closed TEM calculated using an empirical approach.

parameters	50 MHz	200 MHz	400 MHz
initial	1.44	1.38	1.73
optimized	1.33	1.12	1.52

Tab. 2. Comparing the values of VSWR of the closed TEM cell for initial dimensions computed according to the empirical relations and for the optimized model.

To determine the parameters of individual modes in CST, the port location had to be moved without tapering (the constant distance of the walls).

During the optimization, the original size of the TEM cell [1], [7] was increased according to the size requirements for the DUT size. The dimensions were scaled up while keeping $b = w$ constant. By increasing the width of the TEM cell w, the operation area was increased as well. The width of the input septum was determined according to [8], and the value was adjusted to achieve optimal results.

The height of the TEM cell b was chosen according to DUT size requirements. The maximum height of the DUT inside the TEM cell was set to $b/6$. The number of half-waves propagating in the cell depends on the length L. Extension of L does not worsen simulation results.

According to ratios recommended to select initial dimensions of the closed cell, simulations were performed and initial ratios were modified by a sweep [1], [4].

The height b and the width w were set to $b = w$ to maintain the square cross-section of the cell. From relations:

- $w/L = 1.25$,
- $w/b = 1.00$,
- $w/s = 1.37$,

we obtain the optimized dimensions of the cell (see Tab. 1). When a fine tuning was applied, dimensions related to the best possible desired properties were achieved.

Table 2 shows the simulated voltage standing wave ratio (VSWR) values for three different frequencies before and after the optimization. The frequencies in Tab. 2 were selected for three areas with high VSWR values.

The main parameters observed in the simulations follow:

- Voltage standing wave ratio (VSWR) ≈ 1;
- Reflection factor S_{11} [dB] < −10 dB;
- Transmission factor S_{21} [dB] ≈ 0 dB;
- Line impedance $Z_0 \approx 50\ \Omega$;

- Critical frequencies of modes;
- Electric field distribution.

The operating frequency ranged from 0.1 to 500 MHz. For the simulations, the frequency solver was used. This solver is optimal because the discretization grid contained more than 16 thousand tetrahedrons in the final design.

To verify the correctness of simulation results, two different numerical models with the same dimensions given in the Tab. 1 were created (see Fig. 2).

- The numerical model *A* was a vacuum model with a septum from the perfect electric conductor (PEC). The boundary conditions were set to *electric* ($E_T = 0$) in all directions. The material was set to PEC in *background properties*.

  The connectors were made of PEC and PTFE, and the acceptable impedance matching of the whole structure was reached.

- The numerical model *B* had *electric* boundaries ($E_T = 0$) in all directions. In the *background properties*, the material was set to *normal*. The walls and septum were made of PEC. The thickness of the walls was set to zero, and the inner material was vacuum. The connectors were identical to those in the model *A*.

  For the model *B*, we obtained the same simulation results as for the model *A* with identical parameter settings.

The modifications were aimed to eliminate unexpected behavior of the materials that could affect the results. Therefore, the TEM cell is modified to simplify the models and reduce potential inequalities.

The critical frequencies of the modes were approached to the values calculated according to [5]. In addition, the characteristic impedance reached 50 Ω as close as possible.

The TEM cell was manufactured according to the parameters of the final model from the simulations. The details are provided in Sec. 4.

4. Manufacturing the TEM Cell

Figure 3 shows differences between designed TEM cells manufactured from galvanized iron sheets and aluminum. Aluminum excels in relative ease of fabrication by welding individual parts and low weight. The disadvantage of the aluminum is its softness and potential oxidation of the material. Therefore, galvanized iron was used as the final material. Galvanized iron is not the subject to strong oxidation and is more affordable. But rivets or other fasteners have to be used to connect parts.

Copper is an ideal material for manufacturing the TEM cell. Copper is characterized by very good thermal and electrical conductivity. Nevertheless, a very high purchase price was the reason why copper was not considered.

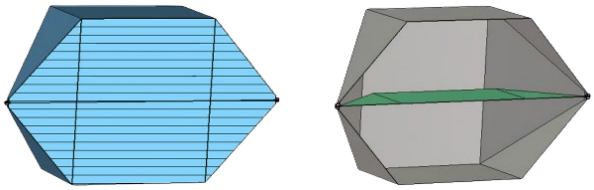

Fig. 2. Two different numerical models were created to verify the simulation results. Left: model A, right: model B.

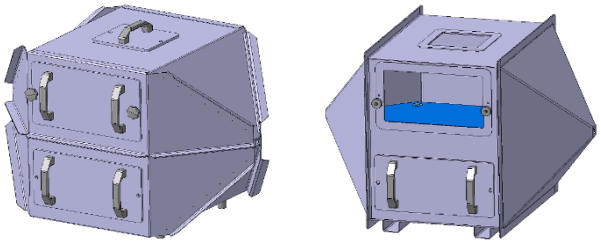

Fig. 3. Designed TEM cells. Left: galvanized iron sheets. Right: aluminum sheets.

For the manufacturing of septum, galvanized iron was used. According to simulations performed, no significant improvement was observed if septum was made of copper.

Three holes were created in the structure to handle the DUT. The top hole is adapted to insert an isotropic field probe that can be used for the verification of measurements.

A handle is attached to each door for better handling. A star nut is used to close the door to the panel. In this way, the door is sufficiently tightened to the panel and no gap is created. A special conductive mesh is inserted to the door to ensure conductive connection between individual mechanic parts. The stability of the construction is ensured by four antivibration rubber feet on the underside of the TEM cell.

As already indicated, the galvanized 1.5 mm thick iron sheet was chosen to manufacture the TEM cell. The individual parts were fixed with galvanized rivets. The lockable door was made of 10 mm thick aluminum with a slit in the groove where conductive elastomer was inserted.

Between two N-connectors (female), a 2 mm thick bulkhead was soldered. The septum was supported by dielectric supports ($\varepsilon_r \leq 1.4$) to hold the septum at a specified height $b/2$. There is a notch in the septum for the center pin of the N-connector, which provides a significantly better impedance matching (see Fig. 4).

A waveguide feedthrough was created for the optical fibres that pass through. The optical fibre was fed into the TEM cell to measure the E-field, control the DUT with the opto-CAN and control the light output on the DUT.

A photograph of the manufactured TEM cell is shown in Fig. 5 and Fig. 8. The DUT was powered by a laboratory power supply coupled to the TEM cell by two 100 nF capacitors. These capacitors were inserted into the panel and were operated as a low-pass filter.

In the following section, measurement results of the manufactured cell are compared with simulations.

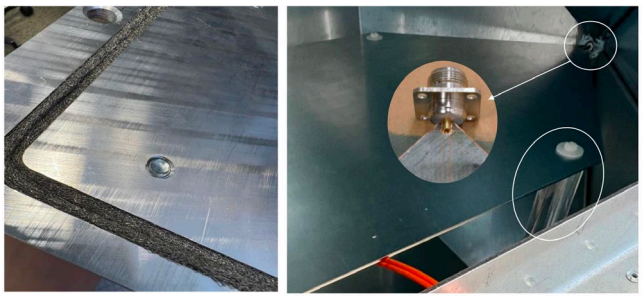

Fig. 4. Dielectric support holding septum at a specified height $b/2$, the notch in the septum for the center pin of the N-connector and slit in the groove where a conductive elastomer was inserted.

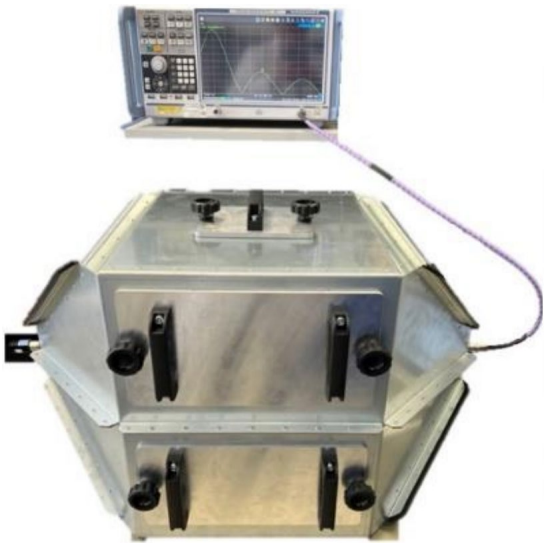

Fig. 5. Photograph of the measured TEM cell.

5. Measurement of the TEM Cell

In Fig. 6, the simulated VSWR characteristics (blue line) and the measured ones (black line) are compared. In experiments, Rohde & Schwarz ZND vector network analyzer (VNA) was used. The VNA was connected to one of two ports, and 50 Ω matching loads (10 W) were connected to other ports.

The agreement between the characteristics is reasonable. Differences in levels were caused by simplifications in simulation models (zero wall thickness, PEC for the conductive part, the material inside the cell is vacuum, etc.). In order to shift simulations towards measurements, a more realistic model of the TEM cell has to be developed:

- Instead of the PEC wall, more realistic models have to be considered;
- Instead of wave ports, more realistic models of connectors have to be taken into account;
- Instead of idealized wall joints, more precise models have to be used.

The CPU-time demands of such a realistic model will be very high and cannot be used for the optimization of the cell.

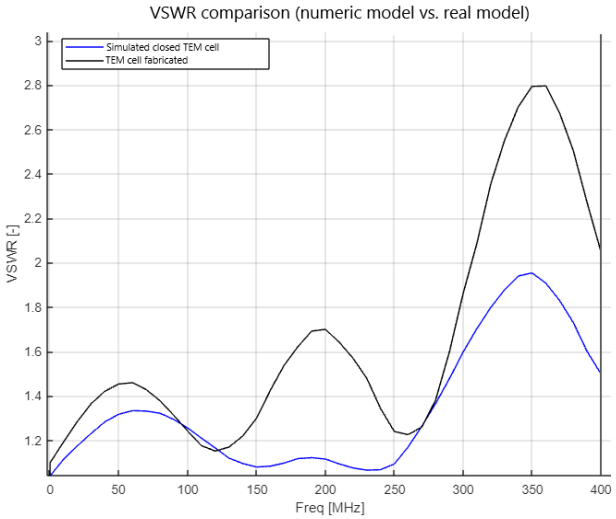

Fig. 6. Frequency response of the VSWR measurement (black) and the simulated one (blue).

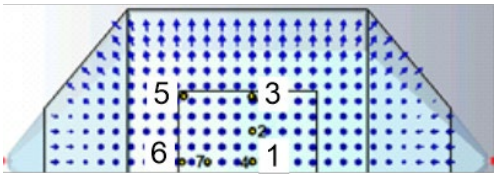

Fig. 7. Specific points above the septum for measurements.

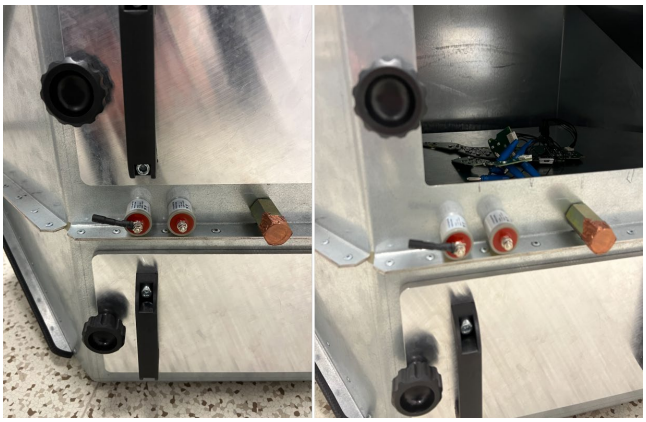

Fig. 8. Photographs of TEM cell with the DUT inserted.

Inside the TEM cell, the E-field was measured at specific points above the septum (h_{DUT}). The points were marked by numbers 1 to 7 (see Fig. 7). First, measurements were performed without the inserted DUT. The isotropic probe for the point no. 3 was in the distance 150 mm from the center (the point no. 1). The distance between the points no. 3 and no. 5 was 150 mm as well.

Due to the symmetry of the structure, the field at opposite points is the same. For the points (–3 : 1 : 3) measured at 65 mm above the septum, the E-field was 36.68 V/m (the amplifier output power was 0.5 W) at 250 MHz.

The final version of the fabricated TEM cell with filtration capacitors and the inserted DUT is shown in Fig. 8.

The DUT is powered by a laboratory power supply. The supply is connected to the DUT inside the TEM cell via

two pass-through capacitors with a capacitance of 100 nF with a maximum current of 16 A (type: FN7513-16-M4). These capacitors are recessed in the panel and behave as low-pass capacitors. For frequencies 10 to 200 kHz, the attenuation is up to 10 dB.

5.1 Electromagnetic Susceptibility

The observed E-field is orthogonal to DUT walls in a specific region inside the TEM cell only (a homogeneous field). Simulations show how the field homogeneity changes when parameters are scaled. A block of vacuum at 0.062 m above the septum corresponds to a DUT maximum size (0.30 m × 0.30 m × 0.10 m). The highest electric field intensity is located at the edges of the septum where the intensity reaches 153 V/m (amplifier output power 0.5 W).

The dependence of the E-field on the probe height is plotted in Fig. 9 for the points indicated in Fig. 7.

Figure 10 shows the frequency dependence of the E-field for different probe positions. The different measurement positions are distinguished by color and numerically marked by 1, 3, 5, and 6. These positions are located at the extreme limits of the maximum allowable DUT size (see Fig. 7). The constant power of the amplifier (40 W) was set and the E-field was measured at a frequency of 100 kHz depending on the position of the probe inside the TEM cell (220 V/m to 245 V/m). With increasing frequency, the E-field difference between probe positions 1 and 5 increases significantly. At 250 MHz, the E-field difference is up to 120 V/m.

In order to test the electromagnetic susceptibility in the chamber, an E-field 200 V/m at 200 MHz is required.

In professional chambers with a TEM cell, biconical antennas are used and the following amplifiers are exploited:

- A biconical antenna amplifier with an output power of 191 W (a logarithmic-periodic antenna)
- TEM cell-amplifier with output power 40 W (Fig. 11).

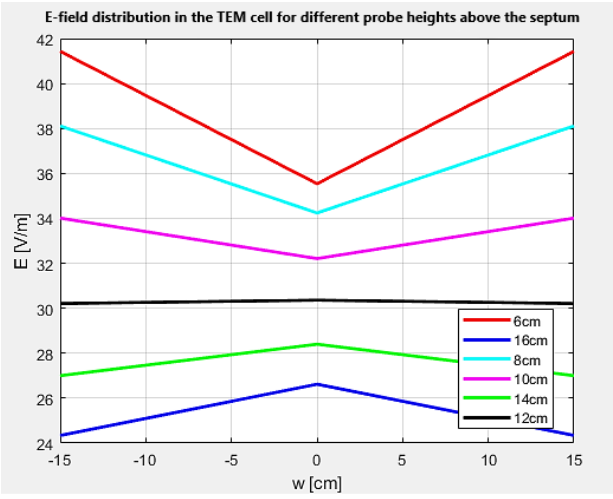

Fig. 9. E-field between points (–3 : 1 : 3) for different heights of the probe (data from simulations).

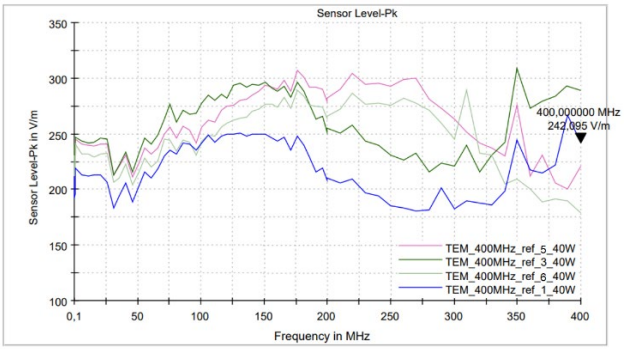

Fig. 10. E-field dependence on frequency for different positions.

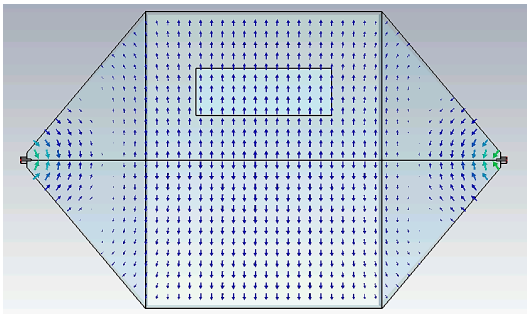

Fig. 11. Side view of the E-field distribution, $f = 250$ MHz.

5.2 Electromagnetic Interference

When interference levels in the TEM cell (Fig. 13) and a professional chamber (Fig. 12) are compared, differences are observed. The professional chamber meets the limits of Class 5, and even more stringent limits given by automotive standards. The TEM cell reaches the limits of Class 3. To meet Class 3 requirements, the average background noise needs to be within 26 dB(μV) for the LW band.

The interferences in a professional chamber appear at the same frequencies as the interferences from the TEM cell.

The interference frequencies detected in the TEM cell measurements were correlated with the measurements in a professional chamber. If a suitable procedure is created to recalculate interference levels between the cell and the chamber, accurate values can be obtained from the cell.

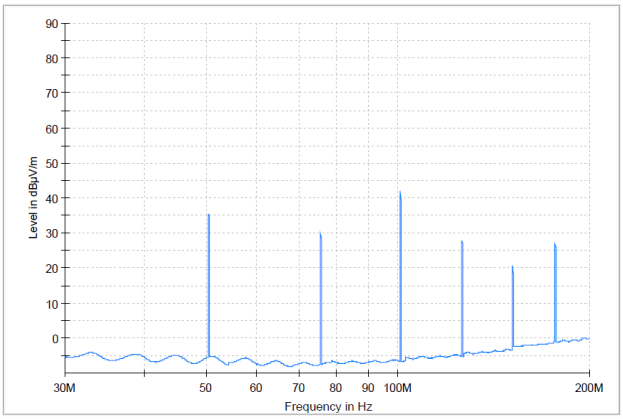

Fig. 12. Interference measurements in a professional chamber (30 MHz–200 MHz), AVG curve.

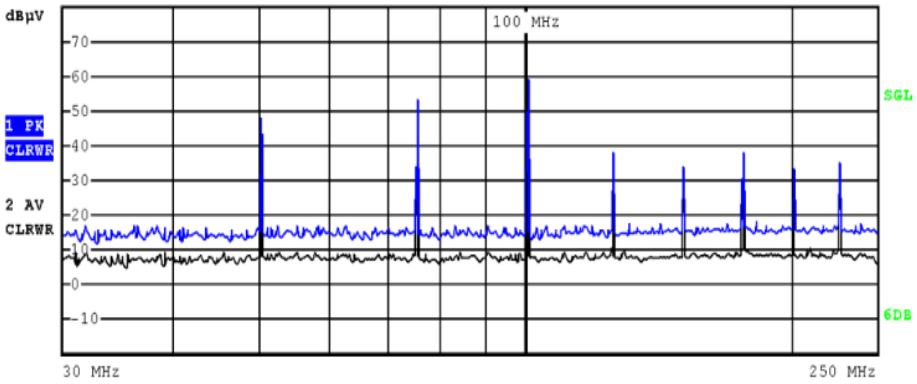

Fig. 13. Interference measurements with an active DUT in a TEM cell (30 MHz–250 MHz), AVG and PK curves.

If the interference level is measured in the TEM cell, this interference will appear in the results from the professional chamber as well (if the test plan is followed).

6. Conclusion

The TEM cell model was simulated in CST Microwave Studio. The operating frequency in the range from 0.1 MHz to 400 MHz allows measurements of devices up to the size of 0.24 m × 0.20 m × 0.06 m (theoretically) and create an electric field with an intensity of up to 250 V/m.

After the detailed analysis, the E-field in the TEM cell design was tested and recalculated for the DUT with size 0.30 m × 0.30 m × 0.10 m ($x \times y \times h_{DUT}$).

Only a single TEM mode has to be excited to make the correct measurements inside the TEM cell. If the frequency exceeds the cut-off frequency of the TEM mode, the relevant TE modes are excited, and a gradual deformation of the field inside the TEM cell starts to appear.

Using the parametric sweep, the model was fine-tuned to obtain the best S-parameters and the 50 Ω matching. The dimensions obtained from the simulations were used to fabricate a TEM cell from 1.5 mm thick galvanized sheet metal, and three closable holes created to handle the DUT.

Differences in final S-parameters of the fabricated TEM cell are caused by real materials and fabrication inaccuracies, but a correlation with the simulations model is apparent. Hence, CST is helpful to design the model, and results can be considered sufficiently accurate.

A TEM cell with a size of 0.80 m × 0.50 m × 0.50 m can be used to measure EMI and EMS. For a constant homogeneous distribution of the E-field in the cell (minimal deviation and best results), a DUT with a maximum size of 0.20 m × 0.20 m × 0.05 m is optimal to be used. Still applicable, it's for maximum DUT size 0.30 × 0.30 × 0.10 m^3.

The TEM cell is a good tool for developing electronic devices in a critical frequency range for measuring electromagnetic immunity and emissions.

Acknowledgments

Research described in this paper was supported by the Internal Grant Agency of the Brno University of Technology under project no. FEKT-S-23-8191.

References

[1] OTT, H. W. *Electromagnetic Compatibility Engineering*. Hoboken (New Jersey): John Wiley & Sons, 2009. ISBN: 978-0470189306

[2] KAISER, K. L. *Electromagnetic Compatibility Handbook*. Boca Raton (Florida): CRC Press, 2005. ISBN: 978-0849320873

[3] CRAWFORD, M. L. Generation of standard EM fields using TEM transmission cells. *IEEE Transactions on Electromagnetic Compatibility*, 1974, vol. 16, no. 4, p. 189–195. DOI: 10.1109/TEMC.1974.303364

[4] DENG, S., POMMERENKE, D., HUBING, T., et al. Mode suppressed TEM cell design for high frequency IC measurements. In *Proceedings of the IEEE International Symposium on Electromagnetic Compatibility*. Honolulu (USA), 2007. DOI: 10.1109/ISEMC.2007.13

[5] MALARIC, K., BARTOLIC, J. Design of a TEM cell with increased usable test area. *Turkish Journal of Electrical Engineering and Computer Sciences*. 2003, vol. 11, no. 2, p. 143–154.

[6] CISPR 12:2007 *Vehicles, Boats and Internal Combustion Engine-driven Devices - Radio Disturbance Characteristics - Limits and Methods of Measurement for the Protection of Off-board Receivers.* CISPR12:2007/AMD1:2009.

[7] CEHN, L., WU, J., ZHENG, Y., et al. Methods to expand the bandwidth of the IC-stripline cell. *IEEE Transactions on Instrumentation and Measurement*, 2022, vol. 71, p. 1–8. DOI: 10.1109/TIM.2022.3208656

[8] GU, Y., LI, D., MA, H., et al. Analysis of higher-order mode effects in the resistively loaded monocone TEM cell. *IEEE Transactions on Electromagnetic Compatibility*, 2022, vol. 64, no. 6, p. 1906 to 1914. DOI: 10.1109/TEMC.2022.3187834

[9] PHAM, H. D., TUTING, K., GARBE, H. Concept to evaluate and quantify field inhomogeneities in coaxial TEM cells. *IEEE Transactions on Instrumentation and Measurement*, 2021, vol. 70, p. 1–14. DOI: 10.1109/TIM.2021.3115214

[10] BOYER, A., BEN DHIA, S. Low-cost broadband electronic coupler for estimation of radiated emission of integrated circuits in TEM cell. *IEEE Transactions on Electromagnetic Compatibility*, 2021, vol. 63, no. 2, p. 636–639. DOI: 10.1109/TEMC.2020.3021135

[11] BUDANIA, M., VERMA, G., JEYAKUMAR, A. Design and analysis of GTEM cell using CST studio simulation. In *Proceedings of IEEE International Conference on Electronics, Computing and Communication Technologies*. Bangalore (India), 2020, p. 1–5. DOI: 10.1109/CONECCT50063.2020.9198456

[12] AMBATI, B. N., BOTSA, V. R., MUNAKA, S. K., et al. Modeling, simulation & validation of TEM cell for short pulse sensor verification. In *Proceedings of 15th International Conference on Electromagnetic Interference & Compatibility*. Bengaluru (India), 2018, p. 1–4. DOI: 0.1109/INCEMIC.2018.8704627

[13] AL-HAMID, M., HEIDEMANN, M., GARBE, H. A novel approach to identify higher order modes in TEM cells. In *Proceedings of IEEE International Symposium on Electromagnetic Compatibility*. Istanbul (Turkey), 2003, p. 453–456. DOI: 10.1109/ICSMC2.2003.1428289

[14] ALOTTO, P., DESIDERI, D., FRESCHI, F., et al. Dual-PEEC modelling of a two-port TEM cell for VHF applications. *IEEE Transactions on Magnetics*, 2011, vol. 47, no. 5, p. 1486–1489. DOI: 10.1109/TMAG.2010.2088381

[15] IFTODE, C., MICLAUS, S., BECHET, P., et al. A TEM cell model analysis for radiofrequency dosimetry improvement by computational means. In *Proceedings of 7th International Symposium on Advanced Topics in Electrical Engineering*. Bucharest (Romania), 2011, p. 1–4.

[16] MORIOKA, T. Probe response to a non-uniform E-field in a TEM cell. In *Proceedings of Conference of Precise Electromagnetics Measurements CPEM 2010*. Daejeon (South Korea), 2010, p. 327 to 328. DOI: 10.1109/CPEM.2010.5543818

About the Authors...

Vojtech BEDNARSKY was born in 1997. He received his B.S. and M.S. degrees in Electronics and Communication Technologies from the Brno University of Technology in 2020 and 2022, respectively. He is currently working toward Ph.D. in Electronics and Communication Technologies at the Brno University of Technology. His research interests include antenna design and microwave propagation.

Zbynek RAIDA (born 1967 in Opava) graduated from Brno University of Technology (BUT), Faculty of Electrical Engineering and Communication (FEEC). Since 1993, he has been with the Department of Radio Electronics, FEEC BUT. In 1996–97, he occupied the position of an independent researcher at Laboratoire de Hyperfrequences, Universite Catholique de Louvain, Belgium. As a professor, he was employed at Metropolitan University Prague (2015–19) and University of Defense Brno (2021–22). Since 2023, he has been a system engineer at NXP Semiconductors. His interests are focused on applied electromagnetics, use of artificial intelligence in RF design, Bluetooth localization and Kinetis W microcontrollers.

Jiří DŘÍNOVSKÝ was born in Litomyšl, Czech Republic, in 1979. He received the M.Sc. and Ph.D. degrees in Electronics and Communication from the Brno University of Technology, Brno, Czech Republic, in 2003 and 2007, respectively. His Ph.D. thesis was awarded by Emil Škoda Award in 2007. Since 2006 he has been an Assistant Professor in Electronics and Communication at the Dept. of Radio Electronics, Brno University of Technology. His research activities include selected topics of EMC, EMI measurements, and EMS testing. He is also interested in specialized problems of radiofrequency and microwave measurements.